Denis J. Phares,[1] *Ph.D., Jason K. Holt,*[2] *M.S., Gregory T. Smedley,*[1] *Ph.D., and Richard C. Flagan,*[2] *Ph.D.*

Method for Characterization of Adhesion Properties of Trace Explosives in Fingerprints and Fingerprint Simulations*

REFERENCE: Phares DJ, Holt JK, Smedley GT, Flagan RC. Method for characterization of adhesion properties of trace explosives in fingerprints and fingerprint simulations. J Forensic Sci 2000:45;(4):774–784.

ABSTRACT: The near inevitable transfer of explosive particulate matter through fingerprints makes it possible to detect concealed explosives through surface sampling. Repeatable and well-characterized fingerprint simulation facilitates quantitative comparison between particulate sampling methods for subsequent detection of trace explosive residues. This study employs a simple, but reproducible sampling system to determine the accuracy of a fingerprint simulation. The sampling system uses a gas jet to entrain particles from a substrate and the resulting airborne particles are then aspirated onto a Teflon filter. A calibrated Barringer IonScan 400 ion mobility spectrometer was used to determine the mass of explosive material collected on the filter. The IonScan 400 was calibrated with known masses of 2,4,6-trinitrotoluene (TNT). The resulting calibration curve is in good agreement with that obtained by Garofolo et al. (1994) (1) for an earlier model of the instrument. The collection efficiency of the sampling system was measured for three particle sizes (8.0, 10.0, and 13.0 μm) using spherical polystyrene particles laced with known quantities of TNT. Collection efficiency ranged from less than 1% for the larger particles to 5% for the smaller particles. Particle entrainment from the surface was monitored with dark field imaging of the remaining particles. The sampling system was then applied to two C4 test samples—a fingerprint transfer and a dry Teflon transfer. Over 100 ng of RDX was collected from the dry transfer sample, while less than 1 ng was collected from the fingerprint transfer. Possible explanations for this large difference are presented based on the system calibration.

KEYWORDS: forensic science, trace explosive detection, fingerprints, residues, latent, particle adhesion, particle resuspension, ion mobility spectrometry, simulation

Efforts to detect hidden explosives have taken two approaches: Advanced imaging technologies that seek to detect the bulk material, and direct chemical identification of trace explosives on a person, package or luggage. A number of trace explosive detectors have been developed, and several are now in use for screening luggage and cargo at airports. Gas chromatography with chemiluminescent detection of the NO produced by pyrolysis of nitrate explosives as well as ion mobility spectrometry are being used at many airports. Mass spectrometry systems for trace explosives detection during security screening are under development, as are a variety of other sensor technologies. All of these methods detect vapor-phase explosives.

Most modern explosives have very low vapor pressures at room temperature. Because of that low volatility, small particles of explosive materials that are inadvertently deposited on surfaces remain accessible for long times, but, although high sensitivities have been achieved with many of these instruments, direct detection by gas sampling alone remains extremely difficult. The effectiveness of trace explosives detection can be greatly enhanced by combining the analytical instrument with a sampling system that delivers the particles from the suspect surface directly to the analyzer. Sampling methods include air sampling or vacuuming a surface, blowing air jets onto a surface to dislodge particles or dust, fibers, or skin flakes to which the explosive may be bound, and wiping the surface. Once particles are collected they can be heated to enhance the vaporization of the trace explosives and the system sensitivity.

The efficiency of a system for physical sampling of trace particles on surfaces depends on the nature of the particles and the substrate, the forces that bind the particle to the surface, and the way that the extraction forces are applied to the particles. The crystalline explosive is generally present in a soft, polymeric matrix, making small particles of the explosive quite sticky. They may be bound to a smooth solid surface, or on fibers or skin, both of which may readily release small fragments that may carry the explosive particles to the analyzer. The particle may be deposited directly on the substrate, or it may be bound to the surfaces with oils in fingerprints or other materials. Removal forces may be applied by an air flow or mechanically by wiping with a tissue, brush, or swab. Once a particle is detached from the surface, it may be transferred to the analytical system, either by sampling the air in which an airborne particle is entrained or by physical transfer of the wipe, or it may be lost or may deposit on surfaces that are not subject to direct analysis, possibly including the original surface.

To understand the efficacy of a sampling method, it must be challenged with samples with well-known properties. Ideally, such samples should reproduce the essential features of the trace explosives likely to be encountered in security applications. A major mode of transfer of particulate explosives is in fingerprints, so there has been considerable effort to develop a synthetic fingerprint. It has been noted that the nature of fingerprints produced after handling an explosive vary as successive fingerprints are made, but

[1] Environmental Engineering Science Department, California Institute of Technology, Pasadena, CA.

[2] Chemical Engineering Department, California Institute of Technology, Pasadena, CA.

Received 28 May 1999; and in revised form 15 Oct. 1999; accepted 18 Oct. 1999.

* This work was supported by the Federal Aviation Administration under grant number FAA-93-G-060.

variations with applied force, humidity, and from one person to another remain substantial.

Fox et al. (2) developed a method for producing highly reproducible challenge samples of explosives of interest by applying known quantities of a suspension of the explosive to a substrate. The suspension is made by dispersing the explosive material into the suspension, so crystals of the explosive are incorporated with the size distribution likely to be encountered in real fingerprints produced after contact with the material. Our preliminary investigations of the adhesion of the particles deposited by the prescribed method to glass plates using the aerodynamic extraction procedure described below revealed that the particles were more tightly bound to the surface than particles in fingerprint samples. This enhanced binding may be caused by the film of polymer that is deposited along with the particles. Samples deposited on fibers produced a similar anomaly as the liquid soaked into the fibers. To develop a standard deposit on fibrous substrates, a modified procedure was developed wherein the suspension is first transferred to Teflon and allowed to dry. The dried deposit is then pressed onto the substrate to be tested, mechanically transferring the sample without the associated liquid.

These standard samples represent an important advance toward quantification of trace explosive sampling systems and procedures. The question remains, however, of how well these reproducible samples simulate fingerprints. In this paper, we shall describe a method that can be used to probe one important aspect of this question: What force, or more precisely, what shear stress is required to detach explosive particles from surfaces? A new technique that employs the well-characterized flow of a gas jet impinging normal to a surface to entrain particles from that surface has been adapted to measure the gas-phase shear stress required to detach particles from the surface. The previous experiments in which this system was used to entrain uniformly sized spherical particles have shown that the shear stress is a strong, and well-defined function of the particle size. The particle entrainment apparatus has been augmented by the addition of a sampling system to collect the airborne particles. The particle extraction and collection efficiencies are separately measured using monosized, spherical, TNT-labeled polystyrene particles. The system is then used to examine the entrainment thresholds for particles in fingerprints and dry-transfer samples on glass slides. We begin with a brief discussion of particle adhesion and the approaches to measuring the forces involved.

Particle Adhesion

A quantitative description of the adhesion of a small particle to a surface must account for a complex combination of molecular interactions and mechanical stresses that deform both the particle and the surface to increase the area of contact. Even the simplest case of a spherical elastic particle at equilibrium with a flat, rigid surface has been the source of considerable controversy (3–7) that has only recently approached resolution. Debate about the magnitude of the force that must be applied to detach the particle from the surface and the extent of deformation near the interface has delayed consideration of important complicating factors such as surface roughness. The classical theories of particle adhesion describe equilibrium between the particle and the substrate, and provide estimates of the force required to detach the particle infinitely slowly. The relevance of the equilibrium theories to detachment of viscoelastic particulate or substrate materials has received little attention. It is, therefore, not surprising that little is known about the adhesion of the ill-characterized and nonuniform particulate deposits in fingerprints.

Direct measurement of the adhesion force between a single particle and a substrate is now possible with scanning probe microscopy techniques, but the question of sampling of such particles from a substrate requires examination of how much material is extracted from an ensemble of particles with a range of particle sizes and shapes and, likely, of quantities of fingerprint oils and other materials that will influence the "stickiness" of the particles. To design and validate a standard sample for calibration and evaluation of security systems, one would like to simulate the mechanisms involved in sampling, but to do so quantitatively. The various sampling approaches can be divided into two classes based on the way the forces are applied to the particles: (a) Mechanical forces applied by brushing or wiping; and (b) Aerodynamic shear forces produced by a gas flow along the surface. The former forces will involve a complex interaction between the particles, substrate, wipe material, applied pressure, and wipe velocity. The latter are more amenable to quantification and will be employed here.

The velocity of a gas flowing along a surface varies from a relatively high value far from the surface to zero at the surface due to viscous dissipation. A particle on a surface only senses the gas motion within the distance that the particle extends from the surface, i.e., for a spherical particle to a distance of one diameter from the surface. For the micron-sized particles of interest here, it is not the absolute velocity of the gas that determines the force applied to the particle, but rather the shear stress,

$$\tau = -\mu \frac{dU}{dz} \tag{1}$$

where μ is the gas viscosity, and U and z are the gas velocity and distance from the surface, respectively. Similar applications of shear stress to particles should yield similar detachment behavior for those particles.

The shear stress delivered to a surface by a steady flow, and hence to particles on that surface, decreases with distance in the flow direction as the thickness of the boundary layer in which viscous dissipation occurs increases. Small particles on large objects are small compared to the boundary layer thickness. On this scale, the velocity increases linearly with distance from the surface (see Fig. 1). The shear stress experienced by particles on the surface is related to the rate of increase through Eq 1. The steep velocity gradients (and thus high shear stresses) necessary to entrain small particles are most readily applied by keeping the thickness of the boundary layer small. Historically, the aerodynamic entrainment of dust particles from surfaces has been investigated using turbulent flows (8–12). This approach is valuable, since, in most practical situations, dust entrainment occurs within turbulent boundary layers. The particles are generally confined to the viscous sublayer, a thin

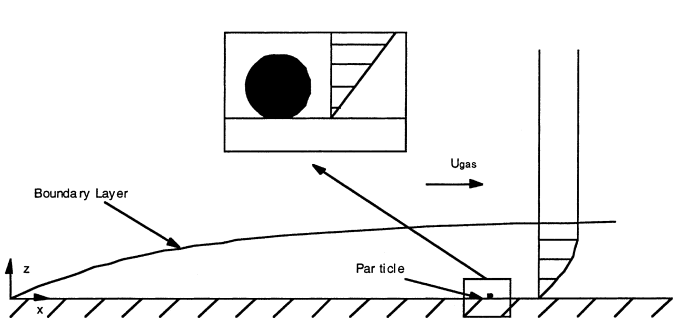

FIG. 1—*Particle within a boundary layer produced by a uniform flow over a flat surface.*

region near the surface in which viscous dissipation dominates. The mean shear rate within this sublayer is, however, thought to be too small to account for the observed entrainment (10). The surface shear rate fluctuates dramatically due to the unsteady nature of the turbulent flow. Energetic turbulent bursts lead to brief high shear events that dominate entrainment in large-scale turbulent flows (8–12). The random nature of these bursts makes it very difficult to quantify the entrainment process, so we seek an alternative approach that will more predictably yield the necessary high shear stress.

Smedley et al. (13) have recently demonstrated that micron-sized particles can be effectively entrained by an impinging gas jet and that, by careful design of the experiment to minimize start-up transients, the threshold for particle detachment can be determined quantitatively. Phares (14) has extended that work to quantify the shear stresses applied by the impinging gas jet. In the present work, we shall use extraction of particles from a surface by an impinging gas jet to infer relative adhesion forces.

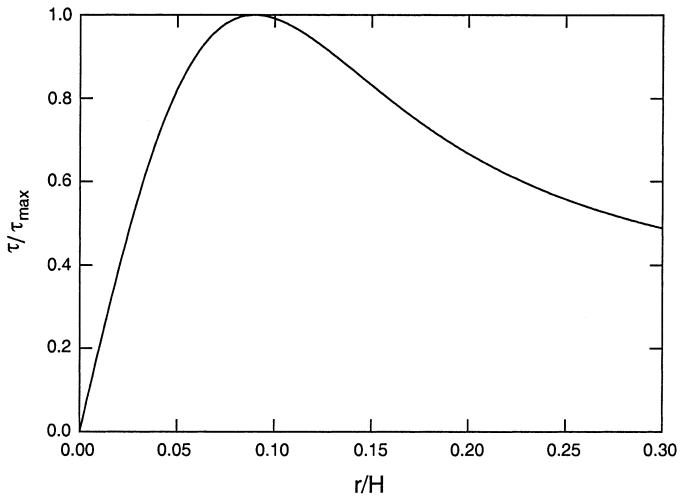

FIG. 2—*Relative shear stress distribution caused by the impingement of a circular jet onto a flat surface.*

The shear stress applied to a surface by a gas jet impinging normally to a surface is zero at the stagnation point (on the center line of the jet), rises to a maximum with increasing radius, and then falls as the boundary layer grows. This behavior is illustrated in Fig. 2 which depicts the radial distribution of the shear stress created by the normal impingement of a circular jet located a height, *H*, from the surface. Not only is the velocity gradient close to the surface sufficient to entrain small particles from the surface, but the shear stress can be unambiguously determined at each radial location.

Several conclusions were drawn from the experiments of Smedley et al. (13) and Phares (14) that are relevant to the sampling of explosive residues from surfaces. First, the shear stress required to induce particle entrainment was found to have at least an inverse cube dependence on particle size. This sensitivity to size is much stronger than predicted by equilibium adhesion theory. Polystyrene spheres smaller than 4 μm in diameter were left untouched by the impinging jet, whereas particles over 12 μm were completely removed from the surface with much smaller jet pressures. Second, they observed that particle detachment is time dependent. The kinetics of particle detachment was found to closely resemble the kinetics of crack propagation through a solid (14), with detachment occuring more rapidly as the imposed force is increased. A consequence of the detachment kinetics is that a larger impulsive force, such as that imposed by an impinging shock wave (15) or an impacting particle (14), is required to detach a particle than would be needed under steady application of the force. Moreover, viscous dissipation at the contact interface during separation slows the detachment of viscoelastic materials, increasing the sensitivity to particle size over that of purely elastic materials.

Experimental

Translating Gas Jet Apparatus

The impinging jet apparatus used to study particle sampling in this study is shown in Fig. 3. The system consists of a computer controlled high speed rail table, a vacuum chuck sample holder de-

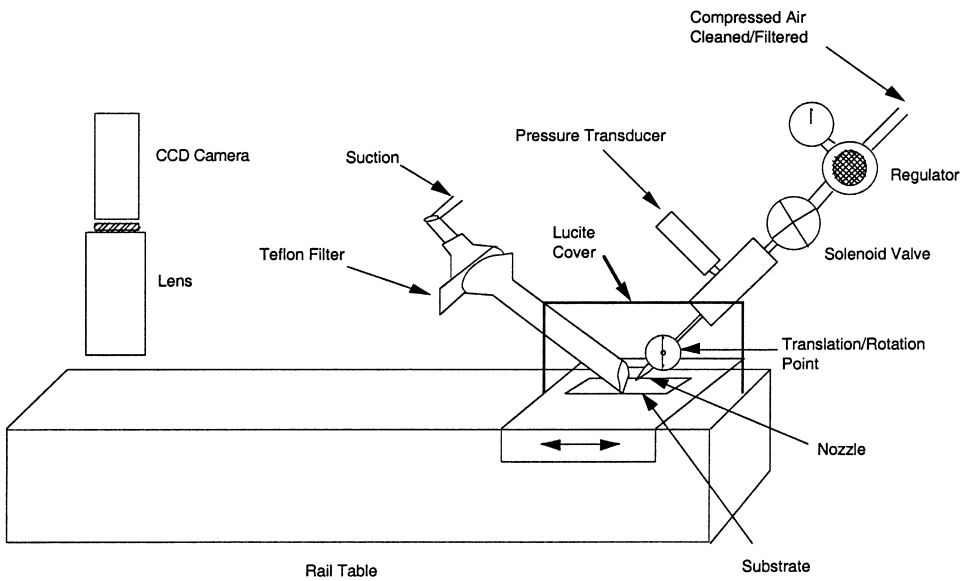

FIG. 3—*Translating gas jet apparatus.*

signed to secure a 25 × 75 mm rectangular substrate, a circular jet nozzle mounted on a rotation stage, and a glass suction tube. The jet nozzle and suction tube are located within a sampling region that is shielded from the laboratory with lucite barriers. The jet pressure is adjusted using a regulator and measured with a Lucas P4100 pressure transducer. Suction is drawn through a glass tube (1.9 cm inside diameter) by a diaphragm pump at a constant flow rate of 40 L/min. A Teflon filter, designed for analysis by the IonScan 400 ion mobility spectrometer, is at the end of the tube 13.5 cm from the suction tube inlet and sealed on both sides with o-rings. The suction tube inlet is flattened into a half circle so that the tube inlet could be lowered close to the jet stagnation zone where particle entrainment occurs. A HeNe laser sheet provides glancing angle illumination of the particles on the substrate, allowing dark field images to be recorded using a CCD camera equipped with a telephoto lens and connected to a Macintosh computer using a Scion LG3 frame grabber card.

Composite Calibration Particle Generation

Monosized spheres made of a polystyrene and TNT mixture were produced in a vibrating orifice aerosol generator (VOAG), specially designed to work with organic solvents (16). A solution of toluene and equal mass amounts of polystyrene and TNT is forced through a small circular orifice, 50 μm in diameter, resulting in fine liquid jet. Breakup of the jet into monosized droplets is induced by sinusoidal vibrations produced by a piezoelectric crystal and transferred acoustically to the orifice through the solution reservoir behind the orifice. The droplets are aerodynamically dispersed and carried in a dry nitrogen sheath flow through a warm drying column, where the droplets dry into smooth, solid spheres of equal size as illustrated in Fig. 4. Attempts to make pure TNT particles from a solution of toluene and TNT resulted in rough and non-spherical particles; so polystyrene was added to the solution to maintain particle sphericity. The final particle size is adjusted by varying the liquid flow rate through the orifice, the solution concentration, and the excitation frequency. The dry spheres are uniformly deposited on cleaned substrates at the bottom of the drying column and subsequently stored in a dry, organic-free environment until use. Three particle sizes were fabricated for this study: 8.0, 10.0, and 13.0 μm. The total mass of TNT in the 8.0, 10.0, and 13.0 μm composite particles was estimated to be 0.17, 0.30, and 0.70 ng, respectively.

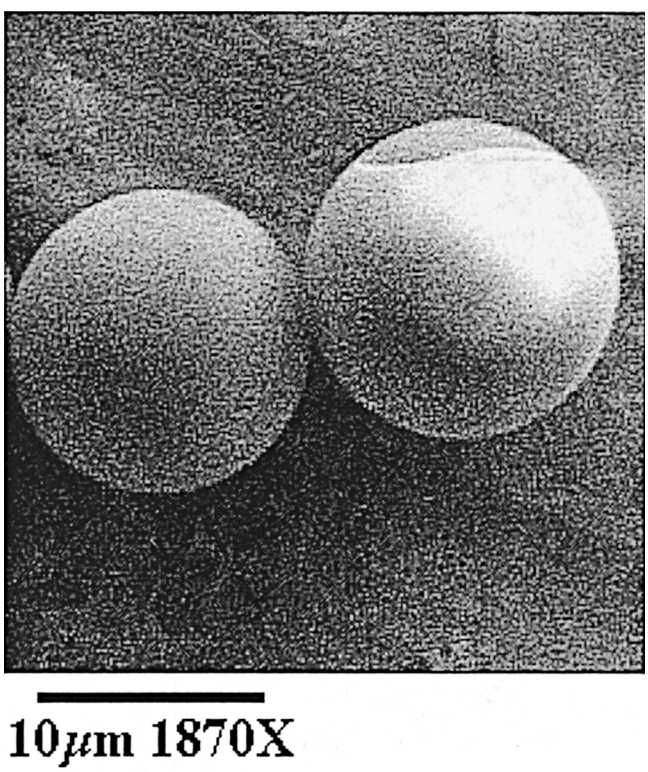

FIG. 4—*Scanning electron microscope image of composite polystyrene/TNT particles at 1870× magnification.*

The substrates used were 25 × 75 mm glass microscope slides. Prior to deposition, the glass slides were thoroughly cleaned with phosphate-free detergent and rinsed with distilled, deionized water. Uniform particle deposits with surface densities of approximately 25 particles/mm^2 were used for the experiments.

Ion Mobility Spectrometer

Chemical detection of the entrained particles was performed by ion mobility spectrometry (IMS). In this technique, atmospheric pressure chemical ionization produces ions from vapor phase analyte molecules. The ions are introduced into a drift tube in a brief pulse. The current detected at a Faraday plate at the end of the drift tube yields the spectrum of ion mobilites.

The IMS used in this study is a Barringer IonScan 400 which has been designed for detection of trace quantities of explosives or contraband in security applications. To quantify the measurements, several modifications to the instrument were required. In normal IonScan 400 operation, mobility analysis is triggered by movement of the filter holder assembly, which is located on a manual translation stage, into the instrument housing. Once the filter is in place inside the instrument, the filter is sealed, the desorber heater turned on, and the drift tube entrance gate pulsed at a frequency of 42 times a second for 20 s. The currents measured within predetermined intervals associated with a peak of interest are added to provide an estimate of the peak area. Thus mobility spectra are being acquired as soon as the desorber heater is turned on. Since all ion detection in the drift tube contributes to the total mass measurement of the initial sample, even the initial spectra acquired while the desorber heater is still heating up are valuable.

In the present study, the movement of the filter assembly was used to trigger the collection of all 840 spectra during the full 20 s of analysis time. Spectra were digitized and stored in a Macintosh computer that was interfaced to the IonScan using a Data Translation Lab NB data acquisition card. To improve the time resolution and peak area determination, the currents from the Faraday plate detector were recorded using an analog-to-digital conversion card on an external Macintosh computer. The peaks were identified and the peak areas above the instrument baseline were measured using the recorded mobility spectra.

Procedure

A clean Teflon filter was analyzed in the IMS, and the explosive peak location was monitored. The cumulative peak area obtained for the clean filter provided the baseline reading for that filter. The filter was then clamped to the end the suction tube, and a test substrate was placed flush with the surface of the translation stage and secured using the vacuum chuck. The stage was moved underneath the CCD camera. A set of images, arranged to cover the entire sampling area, was obtained both before and after the sampling experiment. The size of the sampling area depended on the test sample

used. For the uniform particle deposits generated with the VOAG, a set of three images, spanning 58 mm of the substrate length and 15 mm of the substrate width was necessary to observe the full extent of entrainment. The remaining 23 mm of the substrate length was not exposed to the jet due to size limitations of the rail table. For the fingerprint and dry transfer C4 deposits, only one image was needed to view the entire deposit which was located near the center of the substrate. Each recorded image contained 640 × 480 pixels with 256 levels of gray and was integrated on the CCD chip for a total of 12 frames (0.4 s) to enhance the signal-to-noise ratio. Although the level of magnification (32 μm/pixel) in these images is not sufficient to resolve individual particles, the average pixel intensity of an imaged region is proportional to the particle density within the region.

Once the initial images were recorded, the air jet with a pressure ratio P_{jet}/P_{atm} was started, the suction through the filter was turned on at a flow rate of 40 L/min, and the jet was translated at a constant velocity of 1.8 mm/s under the air jet. Once the sampling region had moved past the air jet, the suction was turned off, and the substrate was returned to the camera location to record the remaining particles on the substrate. Figure 5 displays two close up views of the same area within the sampling region before and after a sampling experiment of 10.0 μm composite particles. The image analysis necessary to determine the number of removed particles is presented in the next section.

Immediately after a sampling experiment, the Teflon filter was removed from the suction tube assembly and placed in the IMS for explosive mass determination. The peak locations for the two types of explosives, TNT and C4, used in this study were determined before the sampling experiments from direct filter deposits of the explosives. This allowed peak area measurements to be performed during analysis of the filter. Nevertheless, all of the obtained mobility spectra were stored in the computer during each filter analysis. In each case, all of the explosive material vaporized from the filter after the first analysis run, and any further analysis yielded baseline level peak areas. Figure 6 displays mobility spectra obtained before and after a sampling experiment on composite particles. Collection of composite particulate material by the Teflon filter is evidenced by the presence of a peak between 12 and 13 ms, corresponding to the mobility of the TNT anions formed in the reaction region of the instrument.

After each sampling experiment, the suction tube was wiped with acetone prior to insertion of a new filter. The translation stage was also wiped with acetone whenever the test sample was changed. A total of 8 test samples were analyzed, including one 8.0 μm, two 10.0 μm, and three 13.0 μm composite particle samples, one C4 fingerprint, and one C4 Teflon transfer sample.

The jet diameter was 0.5 mm, and the jet height, *H*, measured along the centerline of the jet from the jet exit to the sample surface was held constant at 10 jet diameters. Several jet pressure ratios, P_{jet}/P_{atm}, and jet incidence angles, θ, were used in the experiments. Table 1 summarizes the experimental parameters used for each sample.

In order to maximize the number of sampling experiments given the number of test samples, most of the samples were used for multiple sampling experiments. Since samples would be exposed to the jet more than once, multiple experiments were run such that the jet pressure ratio was increased for successive experiments, causing additional particle removal. Calculation of removal efficiency incorporated the number of particles that were already removed in previous runs. Redeposition of particles on the test substrate was observed to be infrequent, and was ignored in the analysis.

Image Analysis

For each sampling experiment, one initial and one final set of images were recorded for further analysis. A comparison between the two image sets provides information about the number of particles that were entrained during the experiment. The initial images of the polystyrene/TNT composite particles contained a nearly uniform distribution of monodisperse particles. During a sampling experiment, particles that pass within a distance of .09*H* from the jet stag-

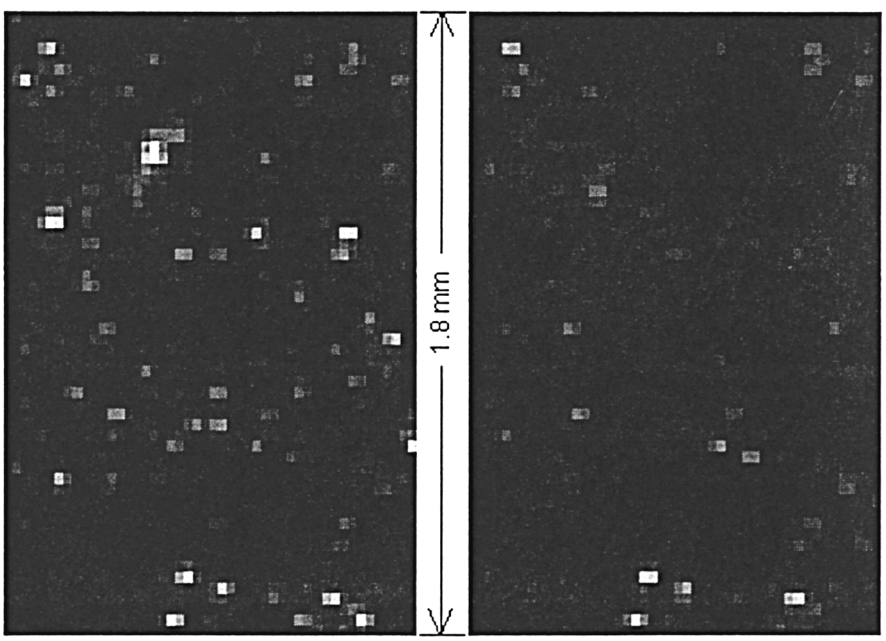

FIG. 5—*Raw images before and after sampling experiment that show removal of 10 μm composite particles.*

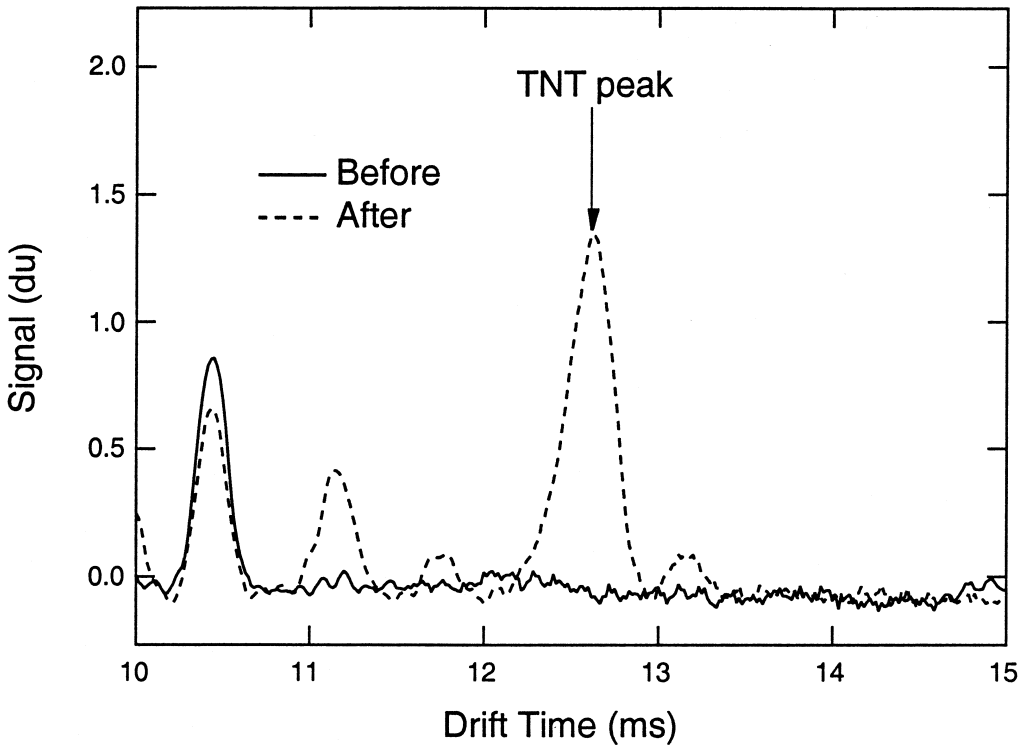

FIG. 6—*Sample mobility spectra obtained from analysis on filter before and after a TNT sampling experiment (1 du = 2.44 mV).*

TABLE 1—*Experimental parameters for test samples.*

Sample	Deposit	θ (degrees)	P_{jet}/P_{atm}
1	13.0 μm composite	90	1.49, 1.84
2	13.0 μm composite	90	1.49, 1.84
3	10.0 μm composite	90	1.49, 1.84
4	8.0 μm composite	90	3.80
5	10.0 μm composite	30	1.49, 1.84, 3.80
6	13.0 μm composite	30, 60	1.49, 1.84, 3.80
7	C4 fingerprint	60	1.84, 3.80
8	C4 dry transfer	60	1.84, 3.80

nation point experience the maximum shear stress imposed by the gas jet (13); and a percentage of these are subsequently removed from the substrate. This causes a decrease in the pixel intensity mainly concentrated in a path of width .09*H*. Since particle removal is constant along the translation axis of the substrate, the pixel intensity, *I*, was averaged for each row of pixels spanning the entire length of the sampling region, yielding one initial and one final average pixel intensity profile. In order to calculate the removal efficiency, the average pixel intensity measured for a clean particle-free glass slide was taken to be the clean pixel intensity, I_0, corresponding to 100% removal. The removal efficiency, η, corresponding to a row of pixels is calculated from the initial and final average pixel intensities from the equation

$$\eta = \frac{I_{\text{final}} - I_{\text{initial}}}{I_0 - I_{\text{initial}}} \qquad (2)$$

where a black pixel has a value of 255 and a white pixel has a value of 0. The same value of the clean pixel intensity, I_0, was used for each sample, as repeated measurements for clean slides yielded variations in pixel intensity of less than 1%. The removal efficiency profile after a single sampling experiment on Sample 2 (13 μ particles, 90° jet incidence, $P_{jet}/P_{atm} = 1.49$) is plotted in Fig. 7 against the closest radial distance, *r*, from the jet stagnation point. The vertical lines denote the boundaries within which particles are exposed to the maximum shear stress imposed by the jet. Note that almost all particle removal occurs in this region. In this particular case, about 30% of the particles present in the high shear stress region before the experiment were removed.

Conversion of removal efficiency to the total number of entrained particles requires a measure of the total number of particles present within the imaged region. Initial particle densities were measured optically to be close to 25 particles/mm^2 and the size of the imaged area is 870 mm^2, yielding 21,750 particles initially in the imaged area. The average removal efficiency, η_{ave}, is calculated from the efficiency profiles (see Fig. 7) and the total number, N_e, of entrained particles is thus given by $N_e = 21{,}750\ \eta_{ave}$.

Due to the wide range of particle sizes and roughness present in the C4 deposits, particle removal is randomly distributed throughout the deposit. Average pixel intensity is no longer proportional to particle surface densities, since the deposited particles do not scatter light uniformly as do monosized spheres. Therefore, quantitative information about particle removal is not attainable from the raw images; only chemical analysis provides quantitative measurements of removal. However, qualitative differences between the two types of deposits may be derived from the images and will be discussed later.

Ionscan 400 Calibration

The IMS was calibrated for quantitative mass determination with known mass amounts of TNT by the method described by

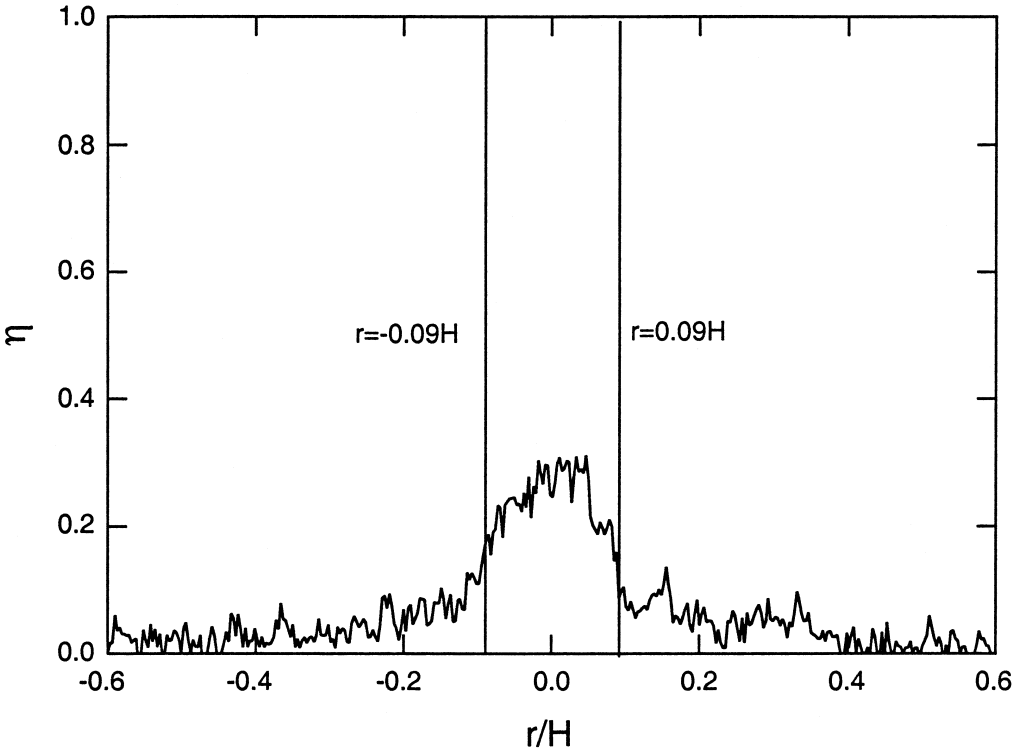

FIG. 7—*Removal efficiency profile from sampling experiment on Sample 2. The vertical lines represent the maximum shear stress boundaries.*

Garofolo et al. (1), with some slight modifications. TNT (obtained from Chem Service, West Chester, PA) containing a minimum of 30% water by weight (quoted 99% pure by the manufacturer) was dehydrated by recrystallization in acetone. HPLC/GC-grade acetonitrile was used to dissolve the TNT in preparing stock solutions. A stock solution with a concentration of 200 ng/μL was prepared, from which subsequent dilutions were used to yield concentrations of 100, 66.7, 33.3, 16.7, 8.33, 4.17, 2.08, 1.04, and 0.52 ng/μL. Further dilution of the 0.52 ng/μL solution as a stock solution yielded concentrations of 0.26, 0.13, and 0.013 ng/μL. These last three solutions are below the range investigated for the previous calibration (1). All of the solutions were made using two Eppendorf 2000 tip ejector pipettes; one was reported to have an accuracy of 1.6% of full scale with a range of 100 to 1000 μL, and the other was reported to have an accuracy of 2.5% of full scale with a range of 10 to 100 μL.

Care was taken to ensure that the same IMS operating parameters were used as in the previous study (1), including the shutter grid pulse width, scan period, delay time, and drift tube temperature. The IMS was placed in bake-out mode for 8 h, prior to the calibration runs to ensure the absence of any contaminants. A standard solution of 1 μL was placed on a clean Teflon filter and allowed to dry for 20 to 30 s before analysis. Typically, 5 to 10 analysis runs were performed for the same concentration, with approximately 1 min between runs to allow the filter to cool to minimize sample vaporization prior to analysis. During a 20 s analysis run, 840 mobility spectra were acquired and sent to a computer through a data acquisition board for analysis of the TNT peak, which was found to lie between 12.34 and 13.06 ms. The peak amplitude, which is given in digital units (1 du = 2.44 mV) by the IMS, was monitored and the cumulative peak area between these limits was determined for all 840 spectra. A clean filter was also analyzed and the cumulative peak area between the same limits was determined and taken to be the baseline value. The baseline was subtracted from cumulative peak areas obtained for all of the analysis runs. The corrected cumulative peak areas and corresponding TNT mass quantities are provided in Table 2.

TABLE 2—*Calibration results for IonScan 400.*

TNT mass (ng)	Cumulative Peak Area (du-ms)
0.013	7661
0.13	10130
0.26	10436
0.52	27496
1.04	28342
2.08	44292
4.17	93894
8.33	100834
16.7	112890
33.3	132454
66.7	151532
100	174128
200	196006

Figure 8 displays the results of the present calibration compared with the results from the previous study (1), where the x-error bars in the present measurements represent the standard deviation determined from repeatability for each solution, and the y-error bars were calculated from uncertainties in the solution concentrations. Results from the previous study were reported as average peak areas and were converted to cumulative peak areas for comparison here. Even though the two studies used different models of the IonScan, there is good agreement in the response of the IMS to sample

mass between the two studies. One particularly noteworthy feature is that both calibrations exhibit a cusp in the IonScan response at around 5 ng of TNT. This is probably an artifact caused by a gain change within the instrument. Two separate exponential fits, also displayed in Fig. 8, were made to describe both sides of the cusp.

The calibration in Fig. 8 allows a calculation of the mass of TNT present on the filter. Determining the number of collected particles from this mass requires knowledge of the mass of TNT in each composite particle. Since baseline levels were achieved after one analysis run of the composite particles, it was assumed that all of the TNT present in the composite particles was desorbed during analysis. The results presented in the next section are based on the assumption that exactly half of the particle mass is TNT. Although further chemical analysis of the composite particles is required to confirm this assumption, the results obtained provide a measure of the collection efficiency, and are therefore sufficient to demonstrate the effect of parametric variation on collection efficiency.

Results

Composite Particles

One disadvantage to performing resuspension and collection experiments with a deposit of monosized particles is that, since there is a strong size dependence on adhesive as well as aerodynamic forces experienced by a particle, removal and collection efficiencies will be either very high or very low. The particle sizes considered in these experiments exhibit very low removal and collection efficiencies, as calculated from image analysis and ion mobility analysis. However, the results obtained for the monosized composite particles, which are summarized in Table 3, exhibit variation with particle size in both removal and collection efficiency.

The effect of particle size on removal efficiency is displayed in Fig. 9. The plot clearly shows that aerodynamic entrainment of smaller particles becomes increasingly difficult, as previous investigations (17) have shown. This result is expected, since

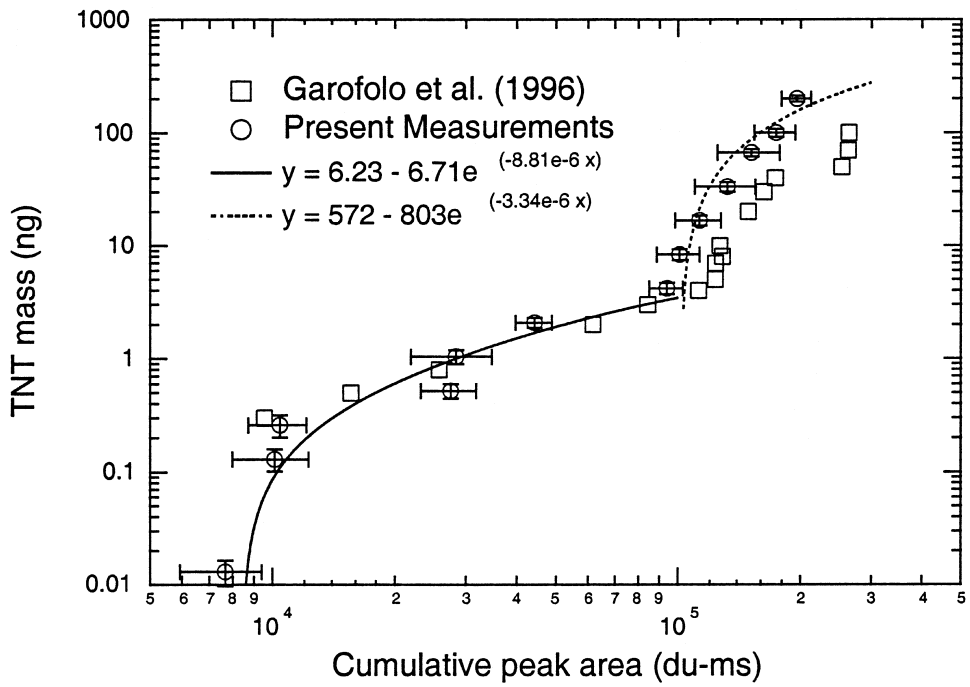

FIG. 8—*TNT mass calibration for two IonScan models.*

TABLE 3—*Experimental results for removal and collection of composite particle test samples.*

Experiment	Sample	Particle Size (μm)	θ (Degrees)	P_{jet}/P_{atm}	Number Entrained	Number Collected	Collection Efficiency %
1	1	13.0	90	1.49	1108	3	.28
2			90	1.84	640	2	.32
3	2	13.0	90	1.49	817	2	.36
4			90	1.84	1178	3	.36
5	3	10.0	90	1.49	704	4	.56
6			90	1.84	163	2	1.3
7	4	8.0	90	3.80	80	4	5.0
8	5	10.0	30	1.49	134	0	0
9			30	1.84	699	0	0
10			30	3.80	1189	1	.08
11	6	13.0	30	1.49	786	1	.12
12			30	1.84	258	0	0
13			60	1.84	147	2	1.4

smaller particles reside deeper within the viscous subplayer of the boundary layer where fluid velocities are small, and the drag experienced by a particle decreases with its surface area. A hyperbolic tangent is fit to the data in Fig. 9 to emphasize that removal efficiency would increase dramatically for particle sizes larger than 13.0 μm.

In contrast, the collection efficiency increases with decreasing particle size due to inertial effects as shown in Fig. 10. Small particles follow the changes of direction of the gas flow more readily than do larger ones. Even though the sampling flow rate (40 L/min) is much greater than the maximum jet flow rate (~1 L/min) inertia limits the entrainment of the larger particles into the sample flow. Larger particles are, therefore, more likely to collide with the suction tube walls or to escape collection entirely.

Figure 11 displays the effect of jet impingement angle on collection efficiency. An important feature of this plot is the low collection efficiency observed for θ = 30°. The length of the region from which particles are entrained doubles as the incidence angle

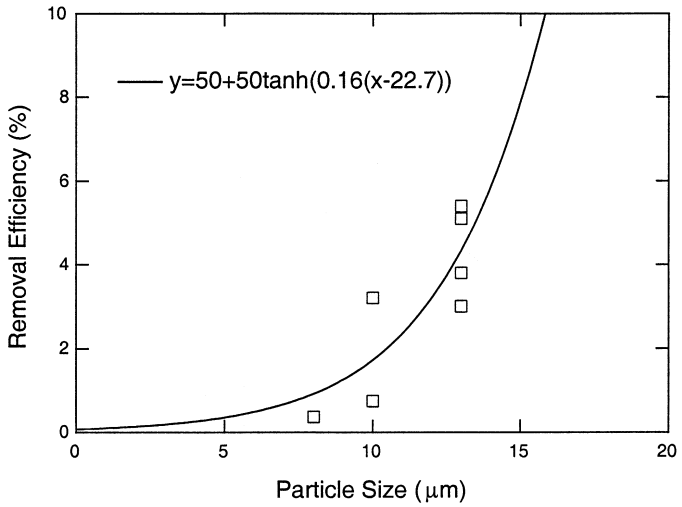

FIG. 9—*Effect of particle size on removal efficiency of composite particles for θ = 90°.*

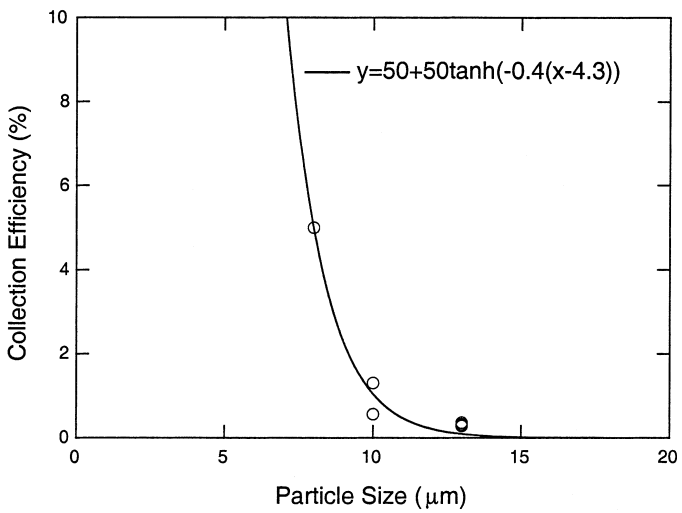

FIG. 10—*Effect of particle size on collection efficiency of composite particles for θ = 90°.*

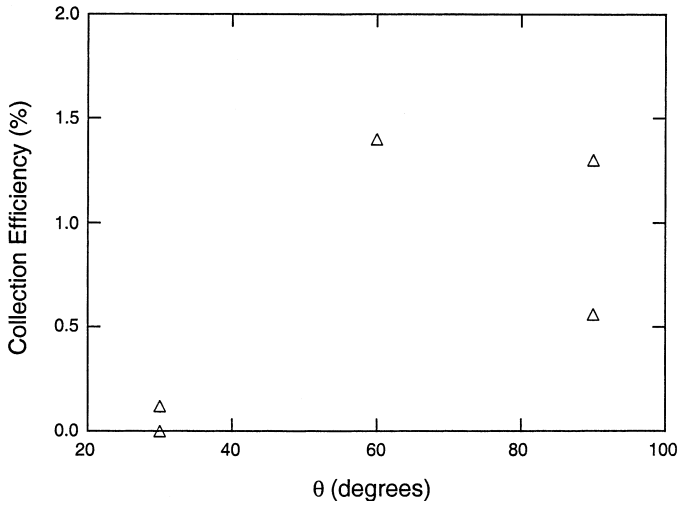

FIG. 11—*Effect of jet impingement angle, θ, on collection efficiency of composite particles for 10.0 μm particles.*

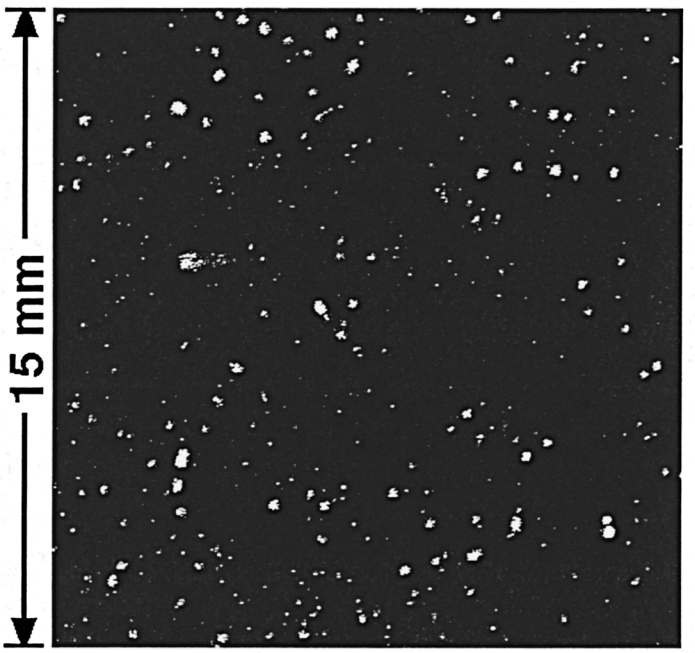

FIG. 12—*Initial raw image of C4 dry Teflon transfer deposit.*

is decreased from θ = 90° to θ = 30°, so it should be possible to collect more material at low incidence angles, but the system will have to be optimized to take advantage of the increased entrainment. Since maximum collection efficiency in the present experiments was observed at θ = 60°, this impingement angle was used for subsequent experiments on the C4 deposits.

C4 Deposits

Figures 12 and 13 display the raw images of the dry Teflon transfer and the fingerprint transfer, respectively. Significant differences are apparent in the size and concentration of the particles present on each substrate. The dry transfer deposit appears to contain smaller numbers of particles than does the fingerprint, but the particles appear to be smaller in the latter deposit. The results of the

sampling experiments on the C4 deposits are summarized in Table 4. For both applied jet pressures, the cumulative peak area obtained from the sampling of the dry transfer deposit is one order of magnitude greater than that obtained from the fingerprint deposit. Although the IMS calibration presented earlier is not expected to hold exactly for C4 due to the difference in molecular weight between TNT and the RDX present in C4, the calibration curve is applied to estimate the relative masses of C4 obtained from both deposits. These results indicate that two or three orders of magnitude more C4 was collected from the dry transfer deposit. Removal images of the dry transfer and fingerprint deposits are displayed in Figs. 14 and 15, respectively, as differences between the final and initial images. Black spots are particles that were removed, while white spots indicate particles that were deposited during sampling, likely redeposition of particles that had been entrained elsewhere on the sample. In light of the removal efficiencies exhibited by the composite particles, it is not surprising that many of the larger particles from both deposits were entrained.

Even though the fingerprint appeared to contain more particles than were present in the dry transfer deposit, more particulate mass was entrained from the latter sample. Since both deposits were exposed to the same aerodynamic shear stress, this result suggests that the particles in the fingerprint adhere to the substrate more strongly than do those in the dry transfer deposit. This is not surprising since capillary forces due to the oils in the fingerprint can significantly increase particle adhesion. It should be noted, however, that although the present results demonstrate the ability to compare particle adhesion in terms of the shear stress required for entrainment of particles from different samples, no quantitative conclusions about the adhesion forces in the two deposit types is possible from just two samples.

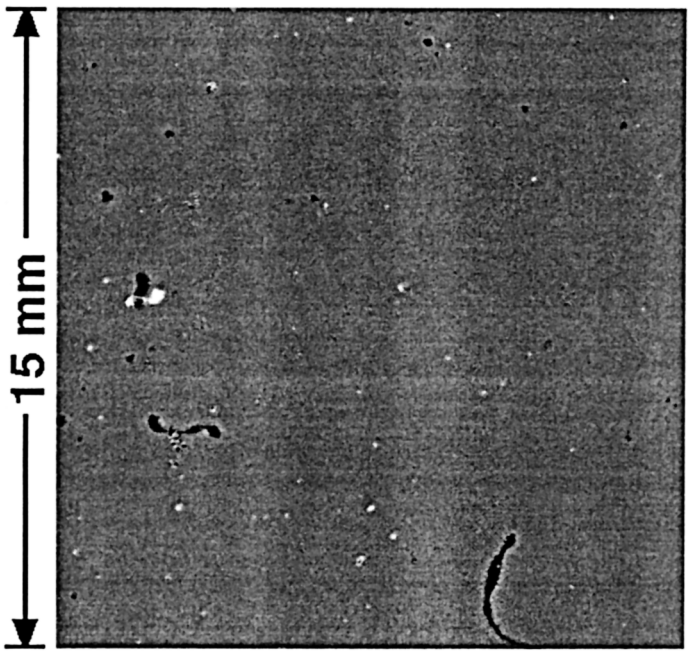

FIG. 14—*Difference between final and initial images of dry transfer deposit.*

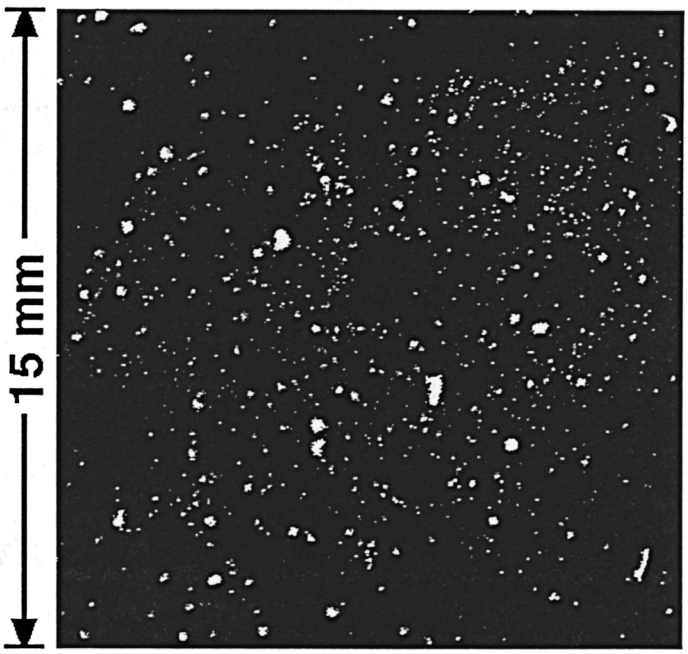

FIG. 13—*Initial raw image of C4 fingerprint deposit.*

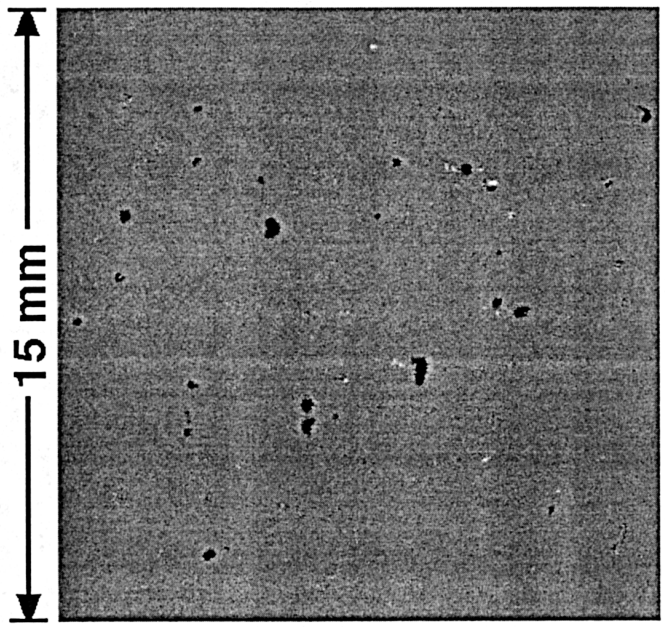

FIG. 15—*Difference between final and initial images of fingerprint deposit.*

TABLE 4—*Experimental results for removal and collection of C4 deposit test samples.*

Sample	Type	P_{jet}/P_{atm}	Cumulative Peak Area (du-ms)	Estimated RDX Mass (ng)
7	Dry transfer deposit	1.84	1.31×10^5	34
		3.80	1.78×10^5	105
8	Fingerprint deposit	1.84	2.00×10^4	0.4
		3.80	1.30×10^4	0.3

Discussion

The present work has demonstrated a system that is capable of subjecting particulate deposits to known aerodynamic shear stresses to study the forces binding micron sized particles of explosives to surfaces. Systematic trends in both the particle removal efficiency and the sample collection efficiency with particle size have been observed for samples consisting of uniformly sized, TNT-laced polystryrene particles. Particle entrainment under the action of steady or long duration shear increases with increasing particle size, as expected given the increase of the applied aerodynamic forces relative to particle adhesion with particle size. In contrast, the aerodynamic sampling decreases in efficiency with increasing particle size as particle inertia impares the ability of the particle to follow the gas motion into and through the sampling system.

Two different samples of C4 were also examined: a C4-laden fingerprint, and a sample produced by a new dry transfer technique, both on clean glass slides. Although more particles were present on the former sample, more were entrained from the latter. Quantitative evaluation of the shear stress required for particle entrainment will require analysis of additional samples in combination with data on the absolute quantities of the explosive in each of the samples. Nonetheless, the two order of magnitude differences between two masses entrained from the two samples demonstrates the feasibility of using aerodynamic entrainment to probe the properties of standard samples. Coupled with direct microscopy-based measurements of the sizes of the particles involved, aerodynamic entrainment could also provide estimates of the actual adhesion forces involved.

The present results also illustrate the possibility of using aerodynamic forces to sample particles from surfaces directly. A small impinging jet imparts much greater shear stresses to a surface than can be achieved with larger air flows that would probe the entire surface of an object that is being screened. The range of particle sizes that is amenable to aerodynamic sampling is limited, however. Previous work (14) has shown that use of transient flows can extend the range of aerodynamic sampling to smaller particle sizes.

Although the present results indicate that the approach of aerodynamic extraction and sampling has merit, there remains considerable room for improvement at larger particle sizes where inertial effects limit the collection efficiency. The sampling system has not been optimized to improve the efficiency of collection of the extracted particles. The observation of low collection efficiency at low jet impingement angles where entrainment is the most efficient clearly indicates that the optimal design of the sampling system is directly related to the approach taken to particle entrainment. The sampling system must be designed to minimize inertial impaction or gravitational deposition of the largest particles to be sampled. An alternate approach would be to ensure that any surfaces on which particles might deposit are hot enough to ensure evaporation so that the material of interest can be delivered to the analyzer.

The present studies were performed using one of the instruments that has been approved by the FAA for security screening in airports. The Barringer IonScan is designed to analyze discrete samples for periods up to 20 s. The detection limit of the instrument is sufficiently low that a small number of micron-sized particles can be detected. A more flexible instrument that allows continuous monitoring of sampled gases could be interfaced to a continuous sampling system to provide a real-time analytical capability.

Acknowledgments

The authors thank Ron Jackson and Lucy May of Barringer Canada for their assistance on interfacing to and calibrating the IonScan 400; and Tom Chamberlain of the FAA Technical Center for developing the dry transfer deposition technique.

References

1. Garofolo F, Marziali F, Migliozzi V, Stama A. Rapid quantitative determination of 2,4,6-trinitrotoluene by ion mobility spectrometry. Rap Comm Mass Spectrom 1996;10:1321–6.
2. Fox FT, Sisk S, DiBartolo R, Green DA, Miller JF. Preparation and characterization of plastic explosive suspensions as analogs of fingerprint derived contaminants for use in certification of explosives detection systems. Federal Aviation Administration, Atlantic City, N.J., 1995.
3. Johnson K, Kendall K, Roberts AD. Surface energy and the contact of elastic solids. Proc R Soc Lond A 1971;324:301–13.
4. Derjaguin BV, Muller VM, Toporov YP. Effect of contact deformations on the adhesion of particles. J Coll Int Sci 1975;53(2):314–26.
5. Tabor D. Surface forces and surface interactions. J Coll Int Sci 1977;58(1):2–13.
6. Muller VM, Yushchenko VS, Derjaguin BV. On the influence of molecular forces on the deformation of an elastic sphere and its sticking to a rigid plane. J Coll Int Sci 1980;77:91–101.
7. Tsai C, Pui DYH, Liu BYH. Elastic flattening and particle adhesion. Aerosol Sci Tech 1991;15:239–55.
8. Corn M, Stein F. Re-entrainment of particles from a plane surface. Am Ind Hyg Assoc J 1965;26:225–36.
9. Vincent JH, Humphries W. The collection of airborne dusts by bluff bodies. Chem Eng Sci 1978;33:1147–55.
10. Wen HY, Kasper G. On the kinetics of particle reentrainment from surfaces. J Aerosol Sci 1989;20(4):483–98.
11. Taheri M, Bragg GM. A study of particle resuspension in a turbulent flow using a preston tube. Aerosol Sci Tech 1992;16:15–20.
12. Braaten DA, Shaw RH, Paw UKT. Boundary-layer flow structures associated with particle reentrainment. Boundary-Layer Meteorology 1993;65:255–72.
13. Smedley GT, Phares DJ, Flagan RC. Entrainment of fine particles from surfaces by gas jets impinging at normal incidence. Exp Fluids 1999;26:324–34.
14. Phares DJ. Particle resuspension from surfaces. Ph.D. dissertation, California Institute of Technology, 1999.
15. Smedley GT, Phares DJ, Flagan RC. Entrainment of fine particles from surfaces by impinging shock waves. Exp Fluids 1999;26(1–2):116–25.
16. Levendis YA, Flagan RC. Synthesis, formation, and characterization of micron-sized glassy-carbon spheres of controlled pore structure. Carbon 1989;27(2):265–83.
17. Liu BYH, Yoo SH, Davies JP, Gresham G, Hallowell SF. Development of particle standards for testing explosive detection systems: characterization of the adhesion between c4 particles and polyethylene. SPIE, 1994;2276:45–55.

Additional information and reprint requests:
Dr. Richard C. Flagan
Professor of Chemical Engineering
California Institute of Technology
Mail Code: 210–41
Pasadena, CA 91125